International Journal of Biological Macromolecules 208 (2022) 995–1008

Contents lists available at ScienceDirect

International Journal of Biological Macromolecules

journal homepage: www.elsevier.com/locate/ijbiomac

Effect of crosslinking strategy on the biological, antibacterial and physicochemical performance of hyaluronic acid and ε-polylysine based hydrogels

Kristine Salma-Ancane [a,b], Artemijs Sceglovs [a,b], Eliza Tracuma [a,b], Jacek K. Wychowaniec [c], Kristine Aunina [a,b], Anna Ramata-Stunda [d], Vizma Nikolajeva [d], Dagnija Loca [a,b,*]

[a] Rudolfs Cimdins Riga Biomaterials Innovations and Development Centre of RTU, Institute of General Chemical Engineering, Faculty of Materials Science and Applied Chemistry, Riga Technical University, Pulka St. 3/3, Riga LV-1007, Latvia
[b] Baltic Biomaterials Centre of Excellence, Headquarters at Riga Technical University, Riga, Latvia
[c] AO Research Institute Davos, Clavadelerstrasse 8, 7270 Davos, Switzerland
[d] Department of Microbiology and Biotechnology, Faculty of Biology, University of Latvia, Riga, Latvia

ARTICLE INFO

Keywords:
ε-Polylysine
Hyaluronic acid
Antibacterial hydrogels

ABSTRACT

The design of multifunctional hydrogels based on bioactive hyaluronic acid (HA) and antibacterial cationic polymer ε-poly-L-lysine (ε-PL) is a promising tool in tissue engineering applications. In the current study, we have designed hyaluronic acid and ε-polylysine composite hydrogel systems with antibacterial and cell attractive properties. Two distinct crosslinking approaches were used: the physical crosslinking based on electrostatic attractions and the chemical crosslinking of charged functional groups (-NH_2 and -COOH). The impact of the crosslinking strategy on fabricated hydrogel molecular structure, swelling behavior, gel fraction, morphology, porosity, viscoelastic properties, antibacterial activity, and in vitro biocompatibility was evaluated. Both chemically and physically crosslinked HA/ε-PL hydrogels demonstrated fast swelling behavior and long-term stability for at least 28 days, as well as similar order of stiffness (10–30 kPa). We demonstrated that physically crosslinked hydrogels inhibited over 99.999% of Gram-negative *E. coli*, while chemically crosslinking strategy led to the antibacterial efficiency decrease. However, cell viability was significantly improved, confirming the importance of the applied crosslinking approach to the antibacterial activity and in vitro biocompatibility. The distinct differences in the physicochemical and biological properties of the developed materials provide new opportunities to design next-generation functional composite hydrogel systems.

1. Introduction

The native extracellular matrix (ECM) is a multimolecular three-dimensional (3D) network made of a large variety of different bioactive polymers, such as peptides, proteins, and glycosaminoglycans (GAGs). It provides the structural and biochemical support for the cells across different tissues types [1–4]. The physically or chemically crosslinked 3D hydrophilic biopolymer matrices, called hydrogels, which can swell by absorbing large amounts of water or biological fluids, are highly attractive tools for mimicking the three-dimensional molecular structure of the native ECM [5]. Hydrogels are innovative biomaterials for tissue engineering, regenerative medicine, and drug delivery applications due to their unique characteristics, such as the ability to encapsulate and release on demand the bioactive compounds (e.g., drugs or growth factors) as well as support the cell proliferation and growth [6–8]. Hyaluronic acid (HA) is an anionic and non-sulfated GAG with unique physicochemical properties and distinctive biological functions. HA, as a critical element of the native ECM, is an attractive building block to design biomimetic cell-interactive hydrogels for local delivery of drugs and cells as well as for tissue bioengineering [3,9,10]. On the other hand, ε-Poly-L-lysine (ε-PL) is an L-lysine based (25–35 L-lysine residues) hydrophilic, cationic homopolyamide which is characterized by biocompatibility, biodegradability, superior tissue adhesive properties, anti-infection and anti-cancer activity and has been

* Corresponding author at: Rudolfs Cimdins Riga Biomaterials Innovations and Development Centre of RTU, Institute of General Chemical Engineering, Faculty of Materials Science and Applied Chemistry, Riga Technical University, Pulka St. 3/3, Riga LV-1007, Latvia.
E-mail address: dagnija.loca@rtu.lv (D. Loca).

https://doi.org/10.1016/j.ijbiomac.2022.03.207
Received 18 October 2021; Received in revised form 21 March 2022; Accepted 30 March 2022
Available online 1 April 2022

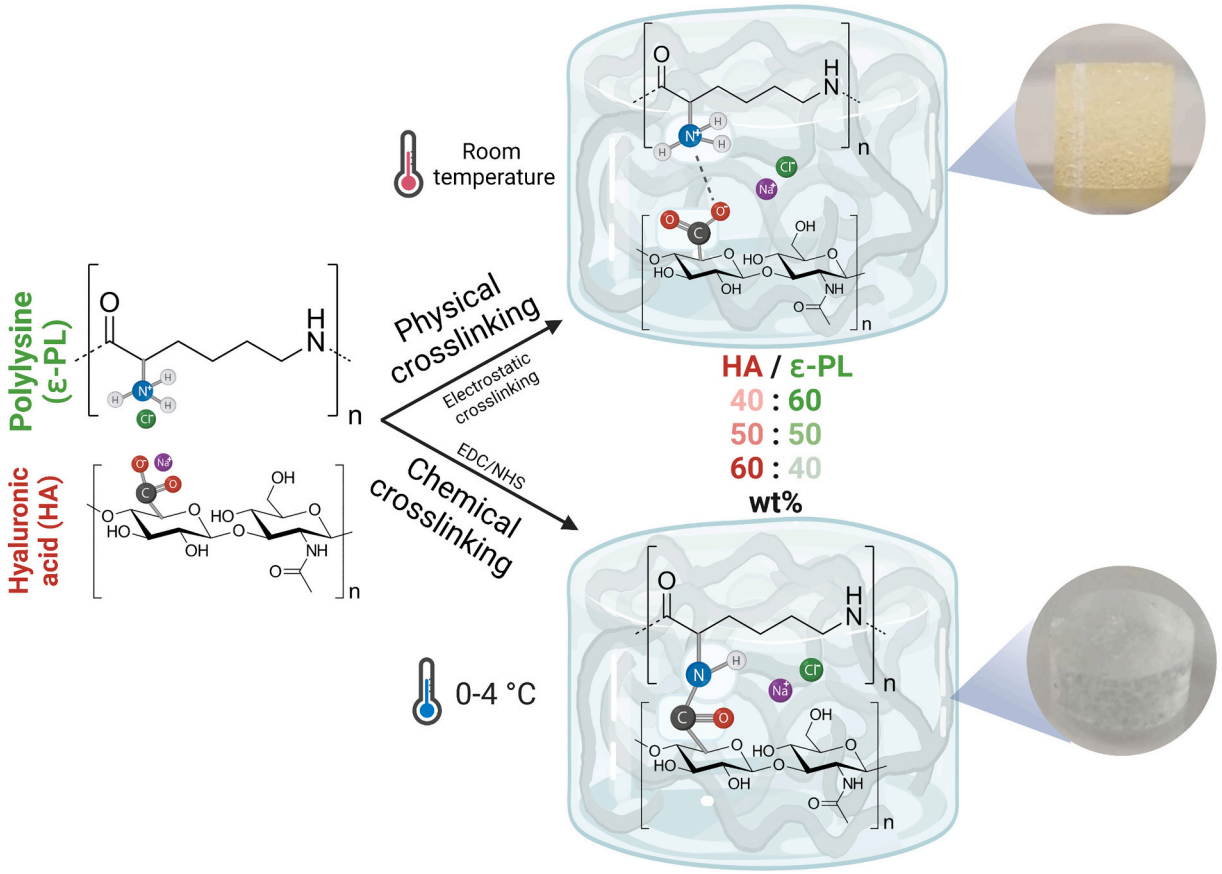

Fig. 1. Schematic illustration of the HA/ε-PL composite hydrogel fabrication process (color).

approved by the Food and Drug Administration in several countries as a commercial food preservative [11–13]. According to the recently reported studies, ε-PL-based biomaterials or hydrogels have shown a great potential to be used in numerous biomedical applications, including antimicrobial agents, targeted drug and gene delivery systems, biological adhesives, and wound healing membranes [12–15]. In the last decade, hydrogels with an anti-inflammatory and antibacterial function have been a research hotspot in the biomedical field [16].

Moreover, such hydrogels must be modified to promote tissue integration before bacterial adhesion. The main challenge is to design antibacterial hydrogels with fast-acting performance and prolonged duration. ε-PL possesses high antimicrobial activity against both Gram-negative (such as *E. coli*) and Gram-positive bacteria (such as *S. aureus*), as well as certain species of fungi and yeast [13,17]. Besides, ε-PL shows strong polycationic property and allows complexation or complementary stacking by electrostatic interactions with anionic polyelectrolytes or polymers [13].

Hydrogels are mainly fabricated using a physical or chemical crosslinking approach or a combination of both methods to build 3D crosslinked polymer networks [18]. The key advantage of the physically crosslinked hydrogels is their biomedical safety, ease of fabrication, and superior biocompatibility. Physically crosslinked hydrogels are usually formed by reversible intermolecular interactions and weak secondary forces, such as ionic/electrostatic interaction, hydrogen bonding, hydrophobic/hydrophilic interactions, crystallization/stereo complex formation, etc., avoiding the use of toxic initiators or chemical catalysts [18,19]. However, physically crosslinked hydrogels present low mechanical properties and limited tunable biodegradation [18,20]. On the other hand, chemically crosslinked hydrogels are usually formed by covalent crosslinking, resulting in better mechanical properties, stability in the physiological environment, and more tunable biodegradation dynamics than the physically crosslinked hydrogels. Up to now, the main chemical crosslinking methods include Michael type-addition, Schiff base formation, Diels-Alder "click" reaction, enzyme-induced crosslink, photo-polymerization [18,21]. Crosslinking strategy is crucial for tissue engineering applications developing hydrogels with desirable physicochemical and biological characteristics [22]. Moreover, hydrogels with the same constituents but different crosslinking structures can present completely different physicochemical performances [18,22].

In the current study, bioinspired and antibacterial composite hydrogels based on the biopolysaccharide HA and polypeptide ε-PL were designed for tissue engineering applications. Physical and chemical crosslinking strategies were chosen for the 3D network hydrogel formation by crosslinks between the carboxyl groups (-COOH) of HA and the primary ε-amino (-NH_2) groups of ε-PL [23,24]. The chemically crosslinked HA/ε-PL hydrogels were fabricated by water-soluble 1-ethyl-3-(3-dimethyl aminopropyl) carbodiimide (EDC)/N-hydroxysuccinimide (NHS) crosslinking. All chemically crosslinked HA/ε-PL hydrogels were prepared with constant EDC/NHS crosslinker concentration and variable HA to ε-PL mass ratio to introduce the non-crosslinked primary amino groups of ε-PL. Antibacterial activity of ε-PL highly depends on its cationic nature. The chemical modification of the cationic primary amino groups on the side chain of ε-PL, which provides excellent antibacterial activity and water solubility, can significantly lower the overall antibacterial activity of prepared hydrogels [14]. The physically crosslinked HA/ε-PL hydrogels were fabricated by complementary electrostatic attraction between two oppositely charged natural polyelectrolytes in the aqueous solution (see Fig. 1) [25–27]. HA acts as an anionic polyelectrolyte and ε-PL as cationic polyelectrolyte, respectively. The key benefits of this crosslinking approach include the green chemistry principles, fast fabrication process

Table 1
Designation and composition of the fabricated HA/ε-PL composite hydrogels.

Designation	Crosslinking method	Composition, wt%	Molar ratio of HA to ε-PL	HA mass (g)	ε-PL mass (g)	Total liquid volume (mL)
Phys HA/ε-PL 40:60	Physical	HA 40 wt%, ε-PL 60 wt%	1:600	0.40	0.60	2.5
Phys HA/ε-PL 50:50	Physical	HA 50 wt%, ε-PL 50 wt%	1:400	0.50	0.50	2.5
Phys HA/ε-PL 60:40	Physical	HA 60 wt%, ε-PL 40 wt%	1:270	0.60	0.40	2.5
Chem HA/ε-PL 40:60	Chemical	HA 40 wt%, ε-PL 60 wt%	1:600	0.21	0.31	4
Chem HA/ε-PL 50:50	Chemical	HA 50 wt%, ε-PL 50 wt%	1:400	0.21	0.21	4
Chem HA/ε-PL 60:40	Chemical	HA 60 wt%, ε-PL 40 wt%	1:270	0.21	0.14	4

in aqueous solutions, injectability for minimally invasive surgical procedures, and the possibility to incorporate the biologically active components [23,28]. However, bulk homogenous polyelectrolyte complex hydrogels are challenging to fabricate due to the inter-molecular flocculation effect between polyelectrolytes with opposite charges [23,29]. In the current study, the suitable experimental conditions for HA to ε-PL mixing, solid to liquid phase ratio, mixing order, and temperature to fabricate homogenous HA/ε-PL hydrogels to prevent inhomogeneous hydrogel formation were investigated.

Moreover, some recent studies have reported that ε-PL containing polyelectrolyte complexes can affect the antimicrobial efficacy of ε-PL as they prevent the cationic ε-PL interactions with the anionic surfaces of the microbial cells [13,30,31]. This study considered fabrication conditions and antibacterial functionality to design physically and chemically crosslinked antibacterial HA/ε-PL hydrogels rationally.

The combinations of HA and ε-PL mainly in polyelectrolyte HA/ε-PL multilayer films [32] and HA/ε-PL composite nanogels have previously been studied [33]. Also, ε-PL in combination with other biocompatible polymers (e.g., chitosan [34], γ-poly(glutamic acid) [26], poly(ethylene glycol) [35]) or bioactive ceramics [36] have been proposed for the antibacterial hydrogel preparation, as well as for drug delivery and tissue engineering [37]. Up to now and to our knowledge, no studies have reported polyelectrolyte complex hydrogels made via amide bond crosslinked hydrogels based on HA and ε-PL. Moreover, unlike polysaccharide-based hydrogels such as HA, relatively few reports have been devoted to polypeptide-based hydrogels such as ε-PL. Therefore, in the current research, our primary objective was to evaluate the physicochemical properties, antibacterial activity, and biocompatibility of bioinspired and antibacterial HA/ε-PL hydrogels as a function of the crosslinking strategy (physical versus chemical). By appropriate choice of the total polymer content, hydrogels in the similar stiffness range were chosen for comparison of the crosslinking methods. Finally we rationalize that by modulating mass ratio of HA to ε-PL, both the physiochemical properties (stiffness and swelling) and antibacterial properties could be tuned. For that, hydrogels with HA to ε-PL mass ratios of 60:40 wt%, 50:50 wt%, 40:60 wt%, corresponding to approximate molar ratios of HA to ε-PL of 1:270, 1:400 and 1:600, respectively, were fabricated. Specifically, by choosing consecutively higher amounts of ε-PL, the total content of the cationic groups typically associated with higher antibacterial activity is expected.

2. Materials and methods

2.1. Materials

ε-Polylysine (ε-PL·HCl, >99% purity, MW 3500–4500 Da, 25–30 L-lysine residues, water content 6.5%) was purchased from Zhengzhou Bainafo Bioengineering Co., Ltd. (China). Sodium hyaluronate (HA, cosmetic grade, >95% purity, water content 13.5%, MW 1.55 MDa) was purchased from Contipro Biotech s.r.o. (Czech Republic). 1-Ethyl-3-(3-dimethyl aminopropyl)-carbodiimide hydrochloride (EDC, 98% purity, MW 191.75 g mol^{-1}, CAS-No: 25952-53-8) was purchased from Novabiochem (USA). N-Hydroxysuccinimide (NHS, 98% purity, MW 115.09 g mol^{-1}, CAS-No: 6066-82-6) was purchased from Sigma-Aldrich. Sodium hydroxide (NaOH, CAS-No: 1310-73-2, ≥99% purity, MW 40.0 g mol^{-1}) and hydrochloric acid fuming (HCl, 37%, ACS, ISO, Reag. Ph Eur) was purchased from Emsure® (Germany). Deionized water (DI) was used throughout this study. All commercially obtained compounds were used as received.

2.2. Synthesis of electrostatically crosslinked HA/ε-PL hydrogels

The physically crosslinked HA/ε-PL hydrogels were fabricated by electrostatic attraction between two oppositely charged natural polyelectrolytes in the aqueous solution (see Fig. 1). The hydrogels were fabricated with HA to ε-PL mass ratio of 40:60 wt%, 50:50 wt%, 60:40 wt% (exact amounts of components are shown in Table 1). Hydrogels were fabricated by mixing 1 g of total polymer content and 2.5 mL of DI water 30 times in two mated syringes. Immediately after mixing, obtained samples were extruded into the custom-made 3D molds (ø = 10 mm) and left at room temperature (23 °C) for 1 h. For in vitro biological studies, prepared samples were sterilized at 105 °C for 4 min in steam under 179.5 kPa using a tabletop pre-vacuum autoclave (ELARA11, Netherlands). Obtained sterile hydrogel samples were kept in a fridge at 4 °C until the use. Prepared hydrogels were removed from the molds for all other experiments, frozen at −26 °C, and freeze-dried using a Martin Christ laboratory freeze dryer (BETA 2-8 LCSplus, Germany) −85 °C for 72 h for further investigation.

2.3. Synthesis of chemically crosslinked HA/ε-PL hydrogels

The chemically crosslinked HA/ε-PL hydrogels were fabricated by carboxyl-to-amine crosslinkers 1-ethyl-3-(3-dimethyl aminopropyl) carbodiimide (EDC) and N-hydroxysuccinimide (NHS) with EDC to NHS molar ratio of 1:1 (see Fig. 1) [38]. The hydrogels were fabricated with HA to ε-PL mass ratio of 40:60 wt%, 50:50 wt%, 60:40 wt% (exact amounts are shown in Table 1). In this case, the HA amount was always kept constant at 0.2095 g, whereas the mass of ε-PL was adjusted accordingly to 0.31425, 0.2095, 0.1397 g. HA was re-dissolved in a 0.25 M NaOH aqueous solution to induce hydrolysis of HA chains and obtain homogenous lower viscosity alkaline HA aqueous solution [39]. The prepared HA solution was rapidly mixed for 10 min at 3000 rpm at room temperature (Vortex V-1 plus, Biosan, Latvia). The HA solution was then left in the dark for 24 h for complete dissolution. Separately, ε-PL was re-dissolved in a 0.25 M HCl aqueous solution and rapidly mixed for 3 min at 1500 rpm at room temperature (Vortex V-1 plus, Biosan, Latvia). To control the gelation speed, after 24 h, the HA aqueous solution was cooled down to ~2 °C by keeping it in a laboratory freezer (−20 °C) for ~12 min (confirmed by repeated temperature measurements). The crosslinking agents, EDC and NHS, were then added to the cooled (4 °C) HA aqueous solution and mixed in by vortexing at 3000 rpm, 1 min for each added crosslinker. EDC/NHS concentration used in this study was 0.24 mol L^{-1} which is considered non-cytotoxic in hydrogel synthesis [26]. Again, separately, the ε-PL aqueous solution was cooled down to ~2 °C by keeping it in a laboratory freezer (−20 °C) for ~12 min (confirmed by repeated temperature measurements). Finally, the HA/ε-PL hydrogels were synthesized by mixing 2 mL of pre-dissolved ε-PL and 2 mL of pre-activated HA aqueous solution containing EDC/NHS in two mated syringes ~200 times (5 min). After mixing, samples were immediately extruded into the custom-made 3D molds (ø = 10 mm) and

left at room temperature (23 °C) for 24 h. For the reaction, the pH of all mixed components, as well as final pH of the fabricated hydrogels was measured and remained in the 5.5–6.5 range. Considering that the efficiency of amide bond formation or amidation in the lasts step in the presence of EDC/NHS is favored at pH 7.5–8 [25], the acidic ε-PL aqueous solution was prepared to neutralize the alkaline HA aqueous solution, resulting in the formation of a neutralization reaction by-product - crystalline phase of NaCl. Indeed, the NaCl phase was detected by X-ray powder diffractometry (XRD, PANalytical X'Pert PRO, Westborough, MA, see Section 2.4.3) in trace amounts (see results in supplementary data Fig. S1). For in vitro biological studies, prepared hydrogel samples were sterilized at 105 °C for 4 min in steam under 179.5 kPa using a tabletop pre-vacuum autoclave (ELARA11, Netherlands). The sterile hydrogel samples were then kept in a fridge at 4 °C until the use. Prepared hydrogels were removed from the molds for all other experiments, frozen at −26 °C, and freeze-dried using a Martin Christ laboratory freeze dryer (BETA 2-8 LCSplus, Germany) −85 °C for 72 h for further investigations. The fabricated HA/ε-PL hydrogel series in this study are summarized in Table 1.

2.4. Physicochemical characterization

2.4.1. Morphology

The surface and cross-section morphology of the lyophilized HA/ε-PL hydrogel samples were visualized by scanning electron microscopy (SEM) Tescan Mira\LMU (*Tescan, Brno, Czech Republic*). Secondary electrons created at an acceleration voltage of 15 kV were used for the sample image generation. The samples were fixed on standard aluminum pin stubs with an electrically conductive double-sided adhesive carbon tape for microscopy. Before examination by SEM, the samples were sputter-coated with a 15 nm thin layer of gold using Emitech K550X (*Quorum Technologies, Ashford, Kent, United Kingdom*) sputter coater. Statistical analysis of the pore size was performed manually from 50 pores per sample across several randomly chosen collected SEM images. The pore shapes were approximated by ellipses, with two radii (the meridian (Y longest) and the equatorial axis (X shortest)) being assigned for each pore, starting from the meridian and then perpendicularly drawing an equatorial line in imageJ©.

2.4.2. Molecular structure

The molecular structure of the lyophilized HA/ε-PL hydrogel samples was investigated by Fourier transform infrared spectroscopy (FTIR) using Varian FTS 800 FT-IR Scimitar Series spectrometer (Varian Inc., Palo Alto, California, USA) equipped with a GladiATR™ monolithic diamond ATR (PIKE Technologies, Madison, Wisconsin, USA). For spectra collection, the lyophilized HA/ε-PL hydrogel samples were grounded into a fine powder using a Mini-Mill PULVERISETTE 23 (*FRITCH, Idar-Oberstein, Germany*) ball mill. The spectra were collected in the mid-infrared range between 400 and 4000 cm^{-1} at a resolution of 4 cm^{-1} by co-adding 50 scans. Background air spectrum with no sample in the infrared beam was acquired before collecting the sample spectrum. Then, the background spectrum was subtracted from the sample spectrum, and the resulting spectra were normalized using Origin 2020 v9.0. Normalization was performed by setting the range 0 to 1 using the default software algorithm, where 1 was assigned to maximum and 0 to minimum values from raw absorbance intensities of all samples.

2.4.3. Phase composition

The phase composition of the lyophilized HA/ε-PL hydrogel samples was evaluated by X-ray powder diffractometry (XRD) using PANalytical X-Pert PRO MPD (Panalytical, Almelo, Netherlands) X-ray diffractometer with a Cu Kα radiation (produced at 40 kV and 30 mA). Diffraction data were collected in a 10–70°2θ range, with a step size of 0.05°2θ and time per step of 2.5 s. Phase's present in the recorded diffraction patterns was identified using a PANalytical X-Pert Highscore 2.2 software (Panalytical, Almelo, Netherlands). For recording of X-ray diffraction patterns, the lyophilized HA/ε-PL hydrogel samples were grounded into a fine powder using a Mini-*Mill PULVERISETTE 23* (*FRITCH, Idar-Oberstein, Germany*) ball mill.

2.4.4. Swelling behavior

The swelling capacity of the freeze-dried HA/ε-PL hydrogels was determined gravimetrically in DI water. The pre-weighted freeze-dried hydrogels were immersed in 20 mL of DI water and incubated under stirring at 100 rpm and 37 °C. The swollen hydrogel samples were weighed at each time interval until 672 h (28 days), removing excess water using filter paper. The corresponding swelling degree was calculated using the following equation:

$$\text{Swelling degree } (\%) = \frac{W_S - W_D}{W_D} \times 100\%$$

where W_S and W_D are the weights of the swollen and initial freeze-dried hydrogel samples, three replicate samples from each prepared hydrogel composition were analyzed, and the results were represented as an average value ± standard deviation.

2.4.5. Gel fraction

The gel fraction of the freeze-dried HA/ε-PL hydrogel samples was determined gravimetrically in deionized (DI) water. The pre-weighted freeze-dried samples were incubated in 200 mL of DI water under stirring at 100 rpm at 37 °C for 48 h. After 48 h, the swollen samples were freeze-dried, and the gel fraction was calculated using the following equation:

$$\text{Gel fraction } (\%) = \frac{W_E}{W_D} \times 100\%$$

where W_D is the initial weight of freeze-dried hydrogels, and W_E is the weight of freeze-dried hydrogel samples after extraction of DI water. Three replicate samples from each prepared hydrogel composition were analyzed, and the results were represented as an average value ± standard deviation.

2.4.6. Oscillatory rheology

The oscillatory rheology measurements were performed on the Physica MCR302 rheometer from Anton Paar. Parallel plate geometry with a 25 mm diameter top plate was used. 2 mm gap was used for the phys HA/ε-PL hydrogels, whereas a 2–2.5 mm gap was used for the chem HA/ε-PL hydrogels. Both phys and chem HA/ε-PL hydrogel samples were pre-prepared in custom-made plastic molds of inner 25 mm diameter and outer 30 mm diameter. Once samples were prepared as described in Sections 2.2 and 2.3, they were immediately placed in molds. For (i) the phys HA/ε-PL hydrogels immediately, and (ii) for the chem HA/ε-PL hydrogels 24 h later, gently placed on the bottom plate using a spatula, and subsequently the top rheometer plate was lowered slowly to minimize hydrogel disruption for each measurement. Prior to taking all measurements, all samples were equilibrated for 180 s. The humidity control hood was used to avoid sample evaporation, and silicon oil was gently spread around the sample directly before each measurement's equilibration. Amplitude sweeps were performed in an oscillatory mode at a constant frequency of 1 Hz at 37 °C, with strain varied from 0.01 to 1000%. Frequency sweeps were then performed in an oscillatory mode from 0.01 to 100 Hz at 0.2% strain within the linear viscoelastic regime, as initially established for all samples during the first amplitude measurements at 37 °C. Each measured point was held at each strain/frequency in both measurements until the instrument reported a stable reading. All measurements were repeated three times to ensure reproducibility.

2.5. Evaluation of antibacterial activity in vitro

In this study, we investigated the antibacterial properties of the

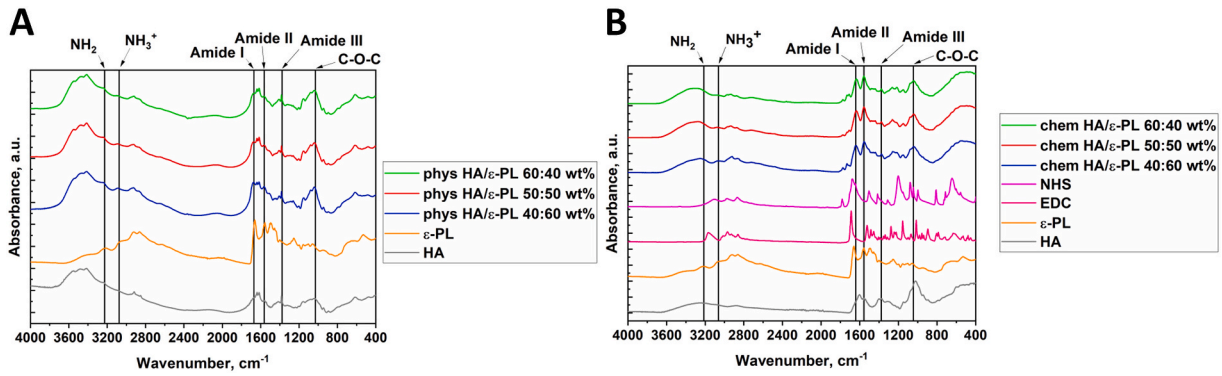

Fig. 2. FTIR normalized spectra of the phys HA/ε-PL (A) and chem HA/ε-PL (B) composite hydrogels. Vertical lines indicate the position of the characteristic bands noted above each line (color).

fabricated HA/ε-PL hydrogels against *Escherichia coli* (*E. coli*) by the zone-of-inhibition test and antimicrobial activity evaluation in bacterial suspension according to ASTM E2149-10. Fresh 18 h shake culture of *E. coli* MSCL 332 grown in a sterile Tryptic soy broth (Biolife, Italy) at 35 ± 2 °C was used in all experiments. Culture was diluted with a sterile 0.3 mM KH_2PO_4 buffer solution (pH 7.2 ± 0.1) until it reached absorbance of $A_{475} = 0.28 \pm 0.02$. This solution was then diluted 1000 times with the buffer to obtain a bacterial working suspension.

2.5.1. Procedure for the determination of leaching antimicrobial presence

Plate count agar (Sanofi Diagnostics Pasteur, France) plates were inoculated with a confluent lawn of bacteria. Eight millimeter diameter wells were bored in the agar medium. Gentamicin (KRKA, Slovenia; 10 mg mL^{-1}, 70 μL) was used as a positive control, and the HA/ε-PL hydrogel samples (diameter 7 mm) were placed in quadruplicate in agar wells. Bacteria were cultivated on an agar medium at 35 ± 2 °C for 24 h. Sterile zones of inhibition were measured using a millimeter-scale ruler.

2.5.2. Procedure for the determination of antimicrobial activity

Each HA/ε-PL hydrogel sample (surface area 3 cm^2) was placed in its tube with 5 mL of bacterial working suspension in potassium phosphate buffer. A series of dilutions were immediately prepared from the inoculum tube without HA/ε-PL hydrogel sample and inoculated into Petri plates on agar media in triplicate to determine the initial bacterial concentration in colony-forming units (CFU) mL^{-1}. All tubes were placed on the shaker at 35 ± 2 °C and mixed at 200 rpm for 1 h ± 5 min. The samples were immediately diluted in triplicate as at the beginning and inoculated into Petri plates with Plate count agar to determine the number of CFU mL^{-1}. Petri plates were incubated at 35 ± 2 °C for 24 h. Colonies were then counted, and the mean CFU mL^{-1} and bacterial reduction were calculated. Log_{10} bacterial reduction = $Log_{10}(B) - Log_{10}(A)$, where A = CFU mL^{-1} for the tube containing HA/ε-PL hydrogel sample after 1 h contact time, and B = CFU mL^{-1} in a tube with inoculum but no HA/ε-PL hydrogel sample after 1 h contact time. Three replicate samples from each prepared hydrogel composition were analyzed, and the results were represented as an average value ± standard deviation.

2.6. In vitro biocompatibility evaluation

2.6.1. Cell culture

BALB/c 3T3 cell line (ATCC) was used for all cytotoxicity assays. Cells were grown in Dulbecco's modified Eagle's medium (DMEM, Sigma) supplemented with 10% (v/v) fetal calf serum (Sigma, USA) and 100 μg $mL^{-1}$of streptomycin, and 100 μg mL^{-1} of penicillin at 37 °C within a humidified 5% CO_2 atmosphere. Cells were detached and passaged using 0.25% (w/v) of trypsin/EDTA (Sigma). For all experiments, cell seeding density was 3×10^4 cells cm^{-2}.

2.6.2. Cytotoxicity assay

The extract test was performed to assess the potentially toxic effects of the hydrogel components. Both cytotoxicities of HA/ε-PL hydrogel extracts and cytotoxicity of ε-PL solutions were assessed. BALB/c 3T3 cells were seeded in 24-well plates and incubated for 24 h to allow them to attach and start proliferating. Hydrogel samples were washed with phosphate-buffered saline (PBS, pH 7.4) and extracted with cell cultivation media (0.2 g hydrogel per 1 mL of cultivation media) for 24 h at 37 °C. Extracts were then collected, diluted with cultivation media to 12.5%, 25%, and 50% (v/v). 0.5 mL of diluted extract was then added to the corresponding cell culture wells of the 24-well plate and incubated for 24 h. Cells incubated without hydrogel samples were used as untreated controls, sodium lauryl sulfate was used as the positive (cytotoxic) control. Phase-contrast microscopy monitored cell cultures, cell confluence, and morphology changes. After incubation, cultivation media was removed, and cells were washed with PBS. Neutral red (Sigma, USA) working solution (25 μg mL^{-1}) in 5% serum-containing cultivation media was added, and cell cultures were incubated for 3 h at 37 °C and 5% CO_2. Neutral red media was removed and extracting solution (1% glacial acetic acid/50% ethanol) was added. After 20 min of incubation at $T = 21$ °C, absorption at 540 nm was measured. Changes in cell viability were calculated using the following equation:

$$\text{Cell viability } (\%) = \frac{\text{Abs}_{540\text{nm}}(\text{treatment}) - \text{Abs}_{540\text{nm}}(\text{background})}{\text{Abs}_{540\text{nm}}(\text{untreated control}) - \text{Abs}_{540\text{nm}}(\text{background})}$$

Five replicate samples of extracts from each phys HA/ε-PL hydrogel composition and at least four replicates of extracts from each chem HA/ε-PL hydrogel composition were analyzed. The results were represented as an average value ± standard deviation.

2.6.3. Direct contact assay

Balb/c 3T3 cells were seeded in 6-well plates and incubated for 24 h. Hydrogel samples were washed three times with PBS and pre-incubated for 1 h in 5 mL of cell cultivation media. Then hydrogels were transferred to cell cultures and incubated for 24 h. After incubation, media and hydrogel samples were removed, and cells were washed with PBS. The neutral red solution was added, and its uptake was measured as described before (see Section 2.6.2. *Cytotoxicity assay*). Cells incubated without samples were used as untreated controls, sodium lauryl sulfate was used as the positive (cytotoxic) control. Phase-contrast microscopy was used to monitor the cell cultures and changes in cell confluence and morphology. Five replicate samples from each prepared hydrogel composition were analyzed, and results were represented as an average value ± standard deviation.

2.7. Statistical analysis

At least three replicate samples from each prepared hydrogel

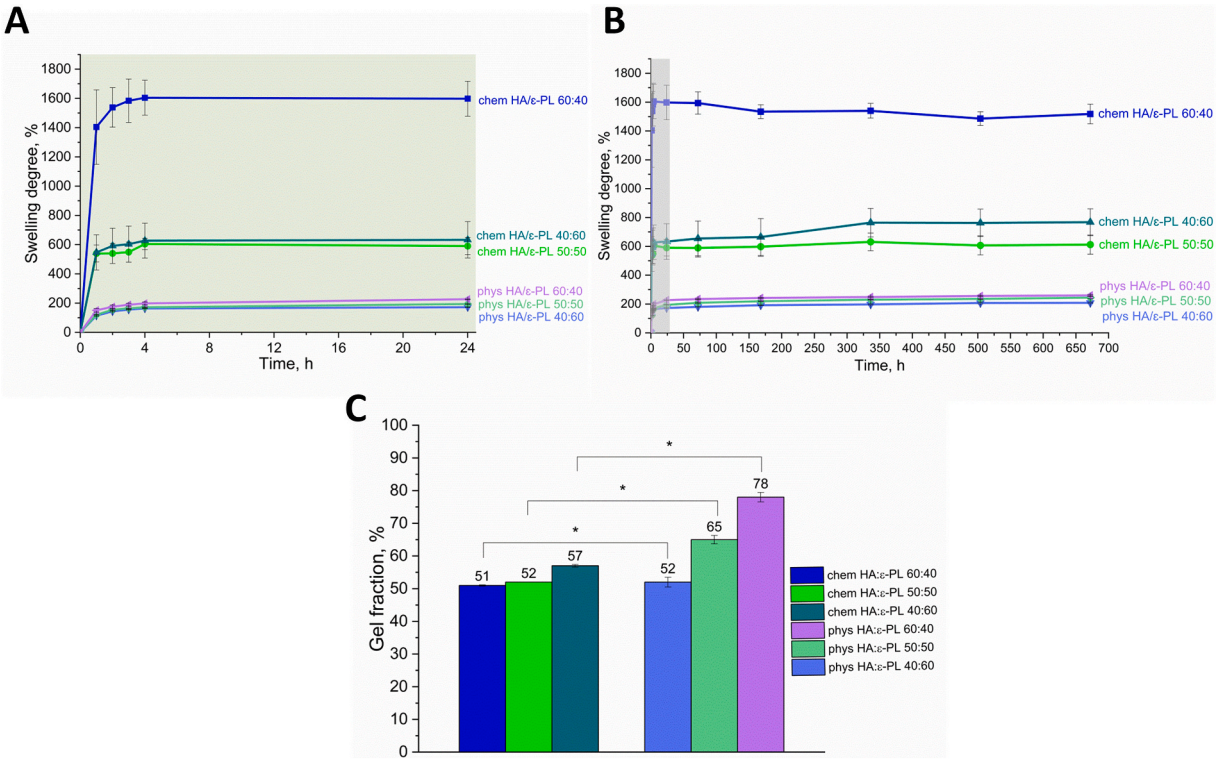

Fig. 3. Swelling degree of the phys and chem HA/ε-PL composite hydrogels (A) up to 24 h and (B) up to 672 h (28 days); (C) gel fraction of the phys and chem HA/ε-PL (color).

composition were analyzed. Average ± standard deviation (SD) was used to express the experimental values. One and two-way analysis of variance (ANOVA) with Tukey's multiple comparison test was used for statistical analysis. A p-value < 0.05 was considered to be statistically significant. (* - for $p < 0.05$; ** - for $p < 0.01$; *** - for $p < 0.001$; **** - for $p < 0.0001$). Curve-fit analysis was performed to calculate IC_{50} for ε-PL. GraphPad Prism 8 software was used for statistical analysis.

3. Results and discussion

3.1. Physicochemical characterization

3.1.1. Molecular structure

To investigate the nature of molecular interactions between HA and ε-PL using physically and chemically induced linkage, FTIR spectra of HA, ε-PL, EDC, NHS, the chem HA/ε-PL hydrogels and the phys HA/ε-PL hydrogels were evaluated (Fig. 2). The FT-IR spectra of HA showed the main characteristic bands as previously reported [40] [41]. The absorption bands at 1640 cm^{-1} (Amide I, C═O stretching vibrations), 1558 cm^{-1} (Amide II, N—H bending vibrations), 1320 cm^{-1} (Amide III), and 1157 cm^{-1} (C-O-C group) were assigned to HA, respectively [40,41]. The absorption bands at 1671 cm^{-1} 1565 cm^{-1}, 1384 cm^{-1} were assigned to the vibrational modes of Amide I (C═O stretching vibrations), Amide II (N—H bending vibrations, C—N stretching vibrations), Amide III bands from ε-PL, respectively [24,42–44]. Given that the Amide I region is also responsible for structural variations in peptides and proteins [45,46], and N—H groups in Amide II region are prone for interactions in our hydrogels, ratio of Amide I/Amide II region taken as I_{1633}/I_{1558} will dictate the type of interactions in the system. Indeed, a clear difference was observed between the types of cross-linking. Increased I_{1633}/I_{1558} ratios of 1.17, 1.33 to 1.35 were obtained for the phys HA/ε-PL hydrogels with HA to ε-PL mass ratios of 40:60 wt %, 50:50 wt%, 60:40 wt%, respectively (Fig. 2A), whereas a similar ratio of 0.87 was obtained for all chem HA/ε-PL hydrogels. The increasing ratio for the phys hydrogels directly corresponds to the mass ratio of HA to ε-PL and suppression of N—H vibrations. On the other hand, in the chem HA/ε-PL hydrogels, irrespective of the ratio of components all side N—H vibrations are suppressed due to the extensive covalent bonding.

Furthermore, the absorption bands at 3246 cm^{-1} and 3081 cm^{-1} were associated with unprotonated NH_2 (secondary amine and primary amine stretching vibrations) and protonated side-chain NH_3^+ groups in solid ε-PL, respectively [24,42,44]. Thus, the ratio between absorbance intensities of these two bands (taken from the normalized spectra (see Section 2.4.2)) is indicative of the overall charge status. NH_3^+/NH_2 ratios of 0.88, 0.83, and 0.78 for the phys HA/ε-PL hydrogels and 0.89, 0.73, 0.65 for the chem HA/ε-PL hydrogels with HA to ε-PL mass ratio of 40:60 wt%, 50:50 wt%, 60:40 wt%, respectively, were calculated from FTIR spectrum (Fig. 2A–B). Higher NH_3^+/NH_2 ratios stand for higher ε-PL content, indicating the higher concentration of free charged NH_3^+ groups. Obtained results revealed that phys HA/ε-PL hydrogels presented a higher free charged NH_3^+ groups content, suggesting other possible differences between phys HA/ε-PL and chem HA/ε-PL hydrogel antibacterial performance.

FTIR spectra of chem HA/ε-PL hydrogels with different HA to ε-PL mass ratios corresponded to the chemical interactions between the molecular structures of ε-PL and HA and formation of the covalent linkage between primary amino groups of ε-PL and carboxylic acid groups of HA via new amide bonds. This was indicated by the shifts in the Amide I, Amide II, and Amide III bands at 1633 cm^{-1}, 1555 cm^{-1} and 1377 cm^{-1}, which correspond to C═O stretching vibration, C═O—NH bond vibration, and C—N bond vibration, respectively [26,42], in comparison to FTIR spectra of pure HA and ε-PL (Fig. 2B). On the other hand, we noted no significant shifts in band positions for any physical HA/ε-PL hydrogels with different HA to ε-PL mass ratios (Fig. 2A).

3.1.2. Swelling behavior and gel fraction

It has been reported that highly swollen hydrogels with high porosity are beneficial for wound healing. They generally provide oxygen transmission, absorb excess tissue exudates, maintain a moist wound

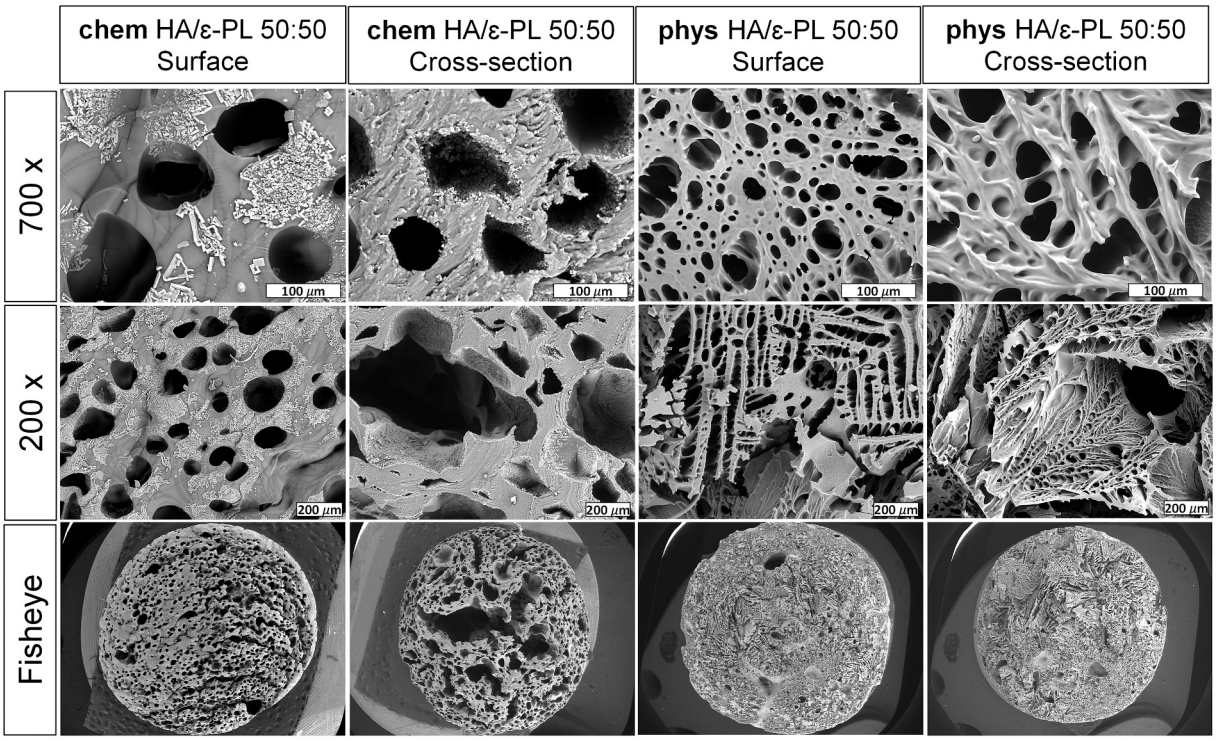

Fig. 4. SEM images of the fabricated phys and chem HA/ε-PL 50:50 wt% composite hydrogels.

environment, and insulate the invasion of external bacteria [47,48]. Hence, swelling behavior is a critical parameter for antibacterial hydrogels, mainly characterized by the swelling or water uptake capacity and the swelling kinetics to reach equilibrium [47]. Both HA and ε-PL have an excellent ability to bind the water molecules due to the highly hydrophilic functional groups in their structure, such as hydroxyl and carboxyl group of HA and primary amino groups of ε-PL [37,49,50]. The swelling degree and kinetics of the phys and chem HA/ε-PL hydrogels were assessed for up to 672 h (28 days) of incubation in DI at 37 °C (Fig. 3A–B). As expected, the crosslinking strategy significantly affected the swelling degree of the fabricated HA/ε-PL hydrogels. In general, the chem HA/ε-PL hydrogels showed a significantly higher swelling degree than the phys HA/ε-PL hydrogels, reaching the maximum at 1600% for chem HA/ε-PL 60:40 (Fig. 3A–B). With the increase of HA content, the swelling degree of the phys HA/ε-PL hydrogels increased slightly and reached 200% (for phys HA/ε-PL 60:40). The phys HA/ε-PL hydrogels exhibited relatively lower swelling degree indicating the formation of dense polyelectrolyte complex hydrogel network based on strong intermolecular electrostatic interactions between ε-PL-NH_3^+···$^-$OOC-HA. This was surprising, considering that the total HA/ε-PL concentration in the phys HA/ε-PL hydrogels was higher than in the chemically crosslinked ones (Table 1). In general, the swelling degree of hydrogels decreases with an increase of crosslinking density; the denser the hydrogel network is, the lower its water uptake capacity and swelling degree [51,52]. Higher swelling degrees of the chem HA/ε-PL hydrogels indicated lower crosslinking density of samples compared to the phys HA/ε-PL hydrogels, or higher porosity, which indeed was confirmed for the chem HA/ε-PL as described in Section 3.1.3. This was also related to the fact that ε-PL can act as a flexible crosslinker between HA chains allowing expansion of the chemically crosslinked network. Both phys and chem HA/ε-PL hydrogels exhibited fast-swelling behavior by reaching the swelling equilibrium within the first 4 h and maintaining equilibrium swelling plateau up to 672 h (Fig. 3A–B). Obtained results revealed the long-term stability and cohesion of the fabricated HA/ε-PL hydrogels under physiological conditions at 37 °C [53], which are essential parameters for functional tissue regeneration applications. Based on the obtained results, all developed HA/ε-PL hydrogels can be classified as superabsorbent or super-swelling materials since they can absorb a high amount of water (>100% of their weight) in a short amount of time [50,54].

The gel fraction of the fabricated HA/ε-PL hydrogels was significantly affected by the crosslinking strategy (Fig. 3C). Obtained results revealed that the phys HA/ε-PL hydrogels have a significantly higher gel fraction than the chem HA/ε-PL ones ($p < 0.05$). In general, the higher gel fraction is associated with a higher crosslinking degree of the hydrogel network. Thus, the phys HA/ε-PL hydrogels with lower swelling degree showed the higher gel fraction values ranged from 52 to 78%, and the gel fraction increased with an increase of HA content in samples. The chem HA/ε-PL hydrogels with higher swelling degree showed lower gel fraction values (~55%) similar for all compositions (differences were statistically insignificant, $p > 0.05$), stemming from the constant EDC/NHS crosslinker concentration used in the hydrogel preparation process.

3.1.3. Morphology

The surface and cross-section morphology of the freeze-dried Phys and chem HA/ε-PL composite hydrogels were visualized by SEM (Fig. 4). SEM images revealed a three-dimensional network with interconnected pores for all hydrogel samples. The homogenous structure was observed in the cross-section images of HA/ε-PL 50:50 wt% hydrogels with pore diameters ranging from equatorial (X) = 65 ± 47 μm to the meridian (Y) = 168 ± 65 μm and for the chem HA/ε-PL hydrogels and from equatorial (X) = 20 ± 9 μm to the meridian (Y) = 35 ± 19 for the Phys HA/ε-PL hydrogels. These trends are in good agreement with the hydrogel swelling behavior suggesting that the high swelling degree is associated with a highly porous hydrogel network, more evident for the chem HA/ε-PL hydrogels if compared to the Phys HA/ε-PL hydrogels (Fig. 3A–B). Furthermore, SEM analysis of the chem HA/ε-PL composite hydrogels revealed the formation of the NaCl crystals on the surface of hydrogels. This observation is consistent with the XRD patterns of the chem HA/ε-PL hydrogels (Fig. S1 in supplementary data). The revealed number and size ranges of pores concur with the desired characteristics of functional

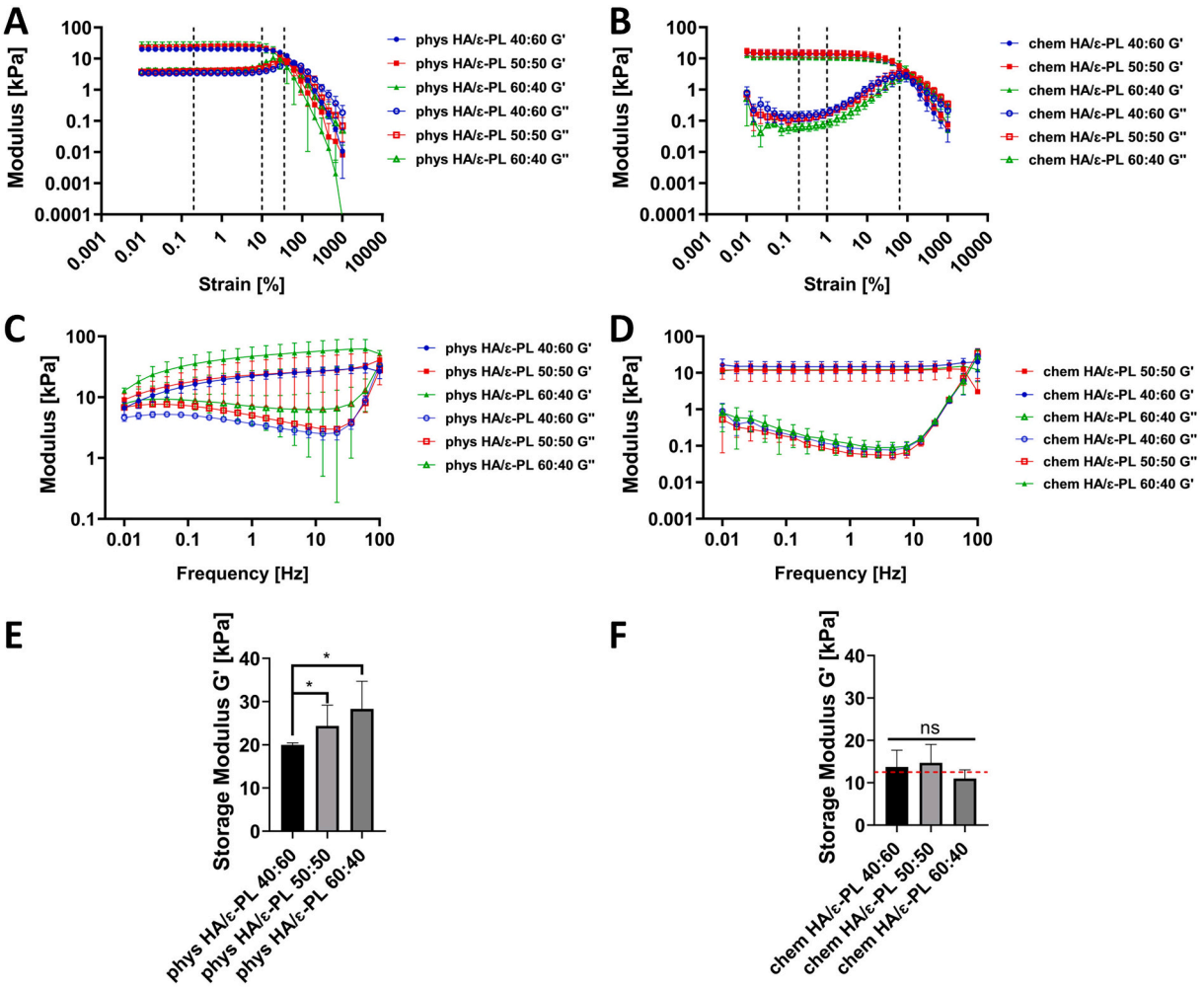

Fig. 5. Oscillatory rheology. Storage (G′ closed symbols) and loss (G″ open symbols) shear moduli vs. strain (ε) curves obtained at 1 Hz frequency of the phys HA/ε-PL (A) and chem HA/ε-PL (B) composite hydrogels. Storage (G′ closed symbols) and loss (G″ open symbols) shear moduli vs. frequency curves obtained at ε = 0.2% strain within the linear viscoelastic region of the phys HA/ε-PL (C) and chem HA/ε-PL (D) composite hydrogels. Extracted mechanical stiffness (Storage modulus, G′) of the phys HA/ε-PL (C) and chem HA/ε-PL (D) composite hydrogels from amplitude sweeps at 1 Hz and 0.2 at ε = 0.2% strain. All data is represented as average ± SD ($n = 3$, * - $p < 0.05$, ns = not significant) (color).

hydrogels for various tissue engineering applications [55,56].

3.1.4. Oscillatory rheology

The oscillatory rheology was performed to assess the mechanical properties of hydrogels. All phys and chem HA/ε-PL hydrogels were initially subjected to an amplitude sweep (Fig. 5A–B). The hydrogel storage shear moduli (G′) was observed to be an order of magnitude larger than the loss moduli (G″), confirming the typically solid-like nature of these hydrogels, irrespective of the chosen crosslinking strategy. All phys HA/ε-PL hydrogels exhibited a well-defined linear viscoelastic region (LVR) until a strain ε ≈ 10% (Fig. 5A). In contrast, the chem HA/ε-PL hydrogels exhibited limited LVR in the range of 0.1–1% strain (Fig. 5B), both marked by vertical dashed lines.

The differences in the mechanical behavior of hydrogels were observed in amplitude sweeps by the considerably different G″ behavior with respect to G′, where for chem gels larger ratio of G′/G″ was obtained at lower strains (indicating more solid-like behavior) but decreasing more rapidly to a crossover point G′ = G″ (compare Fig. 5B to A). The average crossover point has also shifted from ε ≈ 34% to ε ≈ 64% from the phys (Fig. 5A, dashed line most to the right) to chem HA/ε-PL (Fig. 5B, dashed line most to the right) hydrogels, indicating increased resilience to transition from gel to liquid for the chem HA/ε-PL hydrogels, and the ability of ε-PL acting as a flexible crosslinker between HA molecules.

The phys HA/ε-PL hydrogels exhibited behavior similar to the previously reported HA biopolymer solutions/hydrogels [57], where G′ was observed as a function of increased frequency (Fig. 5C). This typical behavior for physically entangled networks had changed for the chem HA/ε-PL, which exhibited a constant G′ across all frequency range (Fig. 5D). In contrast, instead only G″ was affected until a critical frequency of ≈10 Hz, when the transition towards liquid, and indeed hydrogel breaking, started to occur. Although the secondary relaxation time (calculated as a face value of inverse G′ = G″ crossover points in a frequency sweep) is similar for both crosslinking methods and occurs around 100 Hz; the primary relaxation time related to the crosslinking types of networks shifts from phys networks of the order of ~100 s (~0.01 Hz), by approximation and extrapolation at least 2 orders of magnitude to around 10,000 s (~0.00001 Hz) for the chem HA/ε-PL hydrogels, confirming the shift of entangled physical crosslinks to static covalent bonding type of network [58,59].

Finally, we extracted the storage modulus value to give a face value of mechanical stiffness of all hydrogels, a typical approach used for both phys and chem HA/ε-PL hydrogels towards biomedical context [56,60]. For the phys HA/ε-PL hydrogels, a significant increase of stiffness was observed ($p < 0.05$) for the increasing content of HA with G′ of 20 ± 0.5, 24.4 ± 4.8 and 28.3 ± 6.4 kPa, for 40:60 wt%, 50:50 wt%, 60:40 wt%

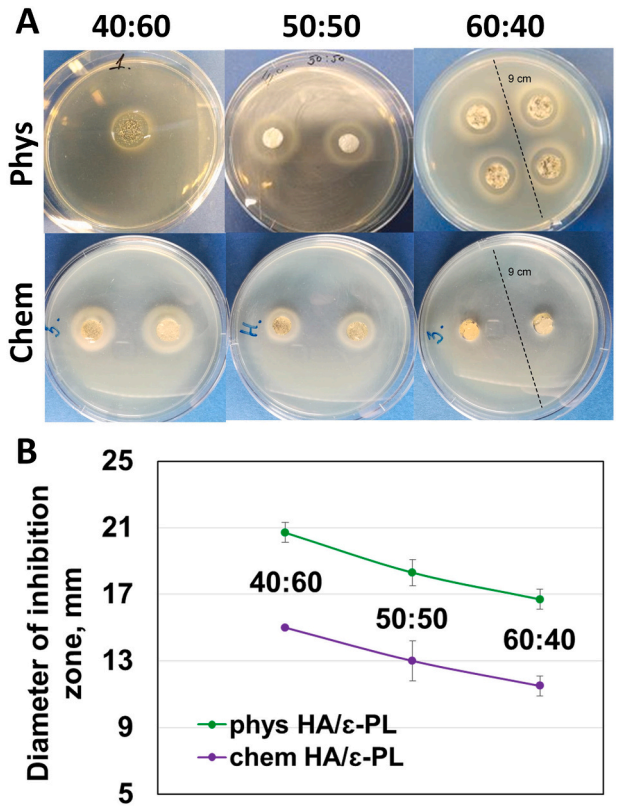

Fig. 6. (A) Representative inhibition zones of the chem and phys HA/ε-PL composite hydrogels and (B) effect of the crosslinking strategy and HA to ε-PL mass ratio on the diameter of the inhibition zone (mm) against *E. coli* (color).

HA to ε-PL mass ratio, respectively (Fig. 5E). On the other hand, irrespective of the ratio, on average, the chem HA/ε-PL hydrogels exhibited 13.2 ± 3.5 kPa G′ value, indicating the dominance of the chemical crosslinks over physical entanglements for this type of crosslinking (Fig. 5F). This is further supported by the fact that the chem HA/ε-PL hydrogels of a total 4-fold lower polymer concentration exhibited similar order of magnitude of stiffness (10–30 kPa) to the phys HA/ε-PL hydrogels. We note that although typically physically crosslinked hydrogels are associated with overall lower stiffness, in our case phys HA/ε-PL hydrogels were prepared at significantly higher HA concentrations (16–24 wt%), making stability dominant over chem gels prepared at 5.25 wt% HA content. Finally, this stiffness range suggests both types of hydrogels could in principle, be used towards e.g., combined antibacterial and musculoskeletal regeneration applications [20], as we will mention in the following sections of this manuscript.

3.2. Evaluation of antibacterial activity in vitro

According to the previous reports, ε-PL peptide shows significant antibacterial activity against Gram-positive and Gram-negative bacteria and fungi [14,61]. In general, the proposed mechanism of antibacterial action is related to the surface of ε-PL which is rich in the cationic amino groups on the side chains and responsible for the antibacterial activity [61–64]. The positively charged cationic amino groups can electrostatically adsorb to the bacteria surface and induce permeabilization of the outer bacterial cell membrane [65,66]. The antibacterial activity of the fabricated phys and chem HA/ε-PL hydrogels was investigated by the zone-of-inhibition test and antimicrobial activity evaluation in bacterial suspension using Gram-negative *E. coli* as the bacterial model organism.

3.2.1. Zone-of-inhibition test

All tested chem and phys HA/ε-PL hydrogels demonstrated antimicrobial activity (Fig. 6) against *E. coli*. The phys HA/ε-PL hydrogels with the same ε-PL mass ratio exhibited significantly ($p < 0.05$) higher antibacterial activity than the chem HA/ε-PL hydrogels, respectively. This stems from: *(i)* the amount of available charged cationic groups on phys HA/ε-PL as confirmed previously by FTIR and gel fraction experiments, *(ii)* total higher polymer content in phys HA/ε-PL, and *(iii)* the fact that the chemical modification directly involves NH_2 groups in the covalent crosslinking impairing exposition of its charge to bacteria. Thus, as expected, the highest activity was observed for phys HA/ε-PL 40:60 with highest ε-PL content and lowest activity for chem HA/ε-PL 60:40 hydrogels with lowest ε-PL content (Fig. 6). As shown in Fig. 6B, the inhibition zone was noticeable in the interface between the phys and chem HA/ε-PL hydrogels and agar, with phys HA/ε-PL hydrogels consistently showing the most significant inhibition of growth. The diameters of inhibition zones increased from 16.7 ± 0.6 to 20.7 ± 0.6 mm for the phys HA/ε-PL hydrogels and from 11.5 ± 0.6 to 15.0 ± 0.0 mm for the chem HA/ε-PL hydrogels with increasing ε-PL mass ratio, respectively.

Table 2
Diameters of sterile zones of inhibition and Log_{10} bacterial reduction after 1 h contact time. The diameter of the agar well was 8 mm. Diameter of sterile zones of inhibition are represented as average ± SD ($n = 3$, * - $p < 0.05$). Log_{10} in a tube with inoculum (without the fabricated HA/ε-PL composite hydrogels) after 1 h contact time was 5.0.

Samples	Diameter ± SD [mm]	Log_{10} bacterial reduction
phys HA/ε-PL 40:60	20.7 ± 0.6*	5.0
phys HA/ε-PL 50:50	18.3 ± 0.8*	5.0
phys HA/ε-PL 60:40	16.7 ± 0.6*	5.0
chem HA/ε-PL 40:60	15.0 ± 0.0*	3.3
chem HA/ε-PL 50:50	13.0 ± 1.2*	2.7
chem HA/ε-PL 60:40	11.5 ± 0.6*	1.8
gentamicin, 10 mg mL^{-1}	30.7 ± 0.6*	–

3.2.2. Antimicrobial activity evaluation in bacterial suspension

Bactericide effect was detected by incubating samples with *E. coli* in liquid under dynamic contact conditions. Log_{10} bacterial reduction after 1 h contact time was 5.0 (Table 2), and the corresponding killing efficiency reached 99.999% for physically crosslinked hydrogels regardless of HA to ε-PL mass ratio tested. The chem HA/ε-PL hydrogels showed significantly ($p < 0.05$) lower antibacterial activity than phys hydrogels. Its value depended on the HA to ε-PL mass ratio in the hydrogel, again confirming that the chemical modification impaired the availability of charged NH_3^+ groups and complementing results from the determination of zones of inhibition in Petri dishes experiments. These results demonstrated that the free primary amino groups of ε-PL are responsible for the antibacterial activity of the fabricated phys and chem hydrogels. Although in principle the formation of HA/ε-PL polyelectrolyte complex in phys hydrogels can affect the cationic interactions of ε-PL with anionic bacteria cells and hinder the antibacterial efficacy, the fabricated phys HA/ε-PL hydrogels maintained the highest antimicrobial activity against *E. coli*. The constant number of primary amino groups of the chem HA/ε-PL hydrogels that are crosslinked via amide bond linkage are not actively affecting bacteria. Instead, only remaining non-crosslinked free amino groups can provide moderate antibacterial effect, which is in good agreement with FTIR results (Fig. 2). In summary, it can be suggested that the fabricated phys HA/ε-PL hydrogels provide a desirable surface charge for high antibacterial activity. Thus, physical crosslinking is a more suitable approach.

3.3. In vitro biocompatibility evaluation

3.3.1. Cytotoxicity of ε-PL

Firstly, ε-PL was tested at concentrations of 3.91 to 125 mg mL^{-1} (Fig. 7A). Among tested concentrations, 7.81 mg $mL^{-1}$and higher were found cytotoxic and decreased the cell viability by more than 90%. In

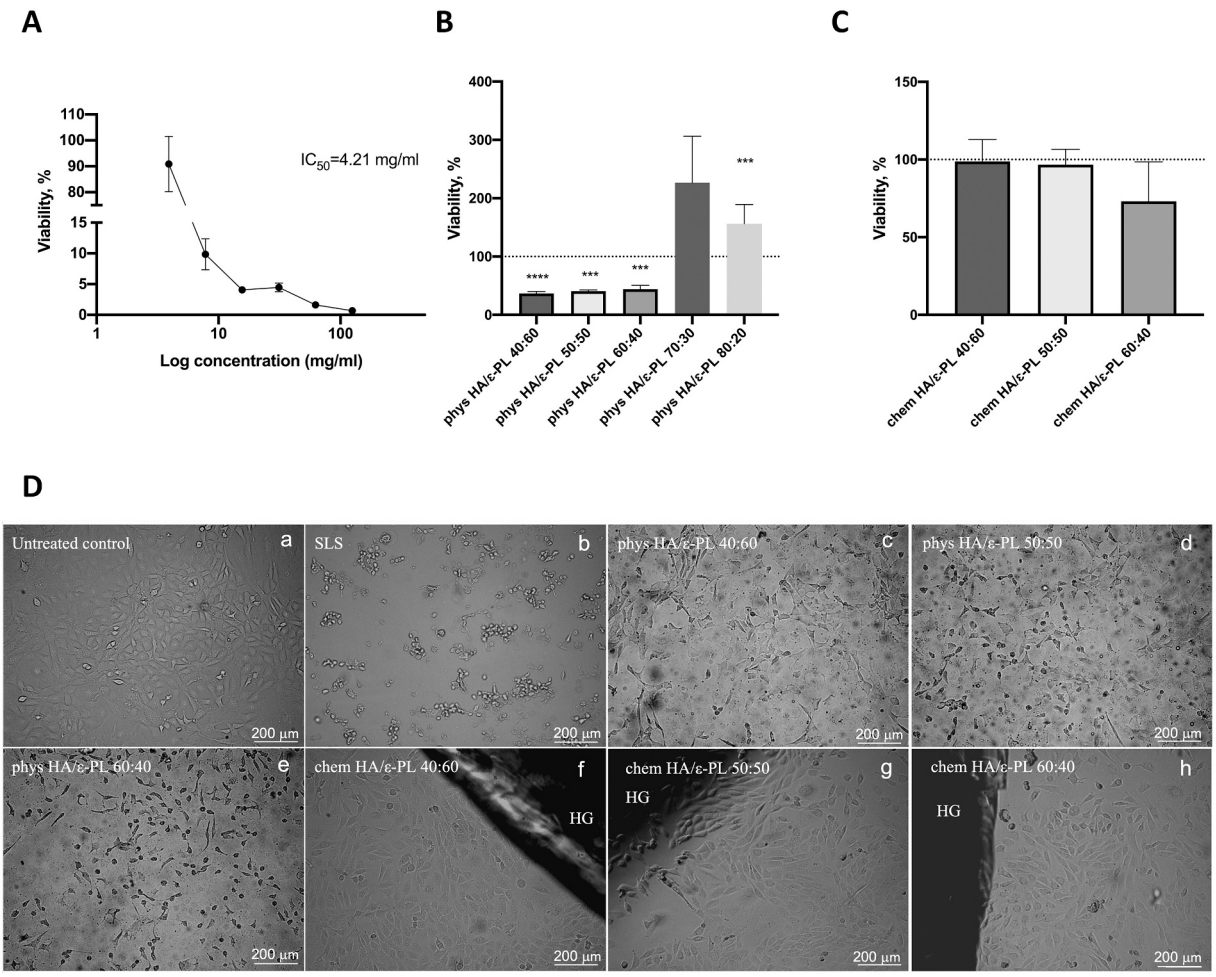

Fig. 7. (A) Cell viability after 24 h of incubation with 3.91–125 mg mL^{-1} ε-PL; (B) direct contact test with the phys HA/ε-PL hydrogel samples; (C) direct contact test with the chem HA/ε-PL hydrogel samples. Dashed lines in the graphs indicate the untreated control level (100%). (D) The representative microscopy images of BALB/c 3T3 cells after 24 h of incubation with the HA/ε-PL hydrogel samples: untreated control (a), cytotoxicity control SLS (b), the phys HA/ε-PL composite hydrogels (c–e), the chem HA/ε-PL composite hydrogels (f–h). For the chem composite hydrogels, the interface between the HA/ε-PL composite hydrogels (HG) and cell monolayer is shown. SLS - sodium lauryl sulfate (cytotoxicity control); $n = 5$; mean ± SD; *** - $p < 0.001$; **** - $p < 0.0001$.

the case of 3.91 mg mL^{-1}, no cytotoxic effects were observed, and cell viability was 90.86 ± 10.65%. Therefore, IC_{50} value for ε-PL was found to correspond to 4.21 mg mL^{-1}. Results are comparable to those observed in other studies. For example, in L929 cell line IC_{50} value (concentration that reduces cell viability by 50%) of ε-PL was 8 mg mL^{-1}, and the toxicity was significantly lower than that of the α-polylysine (α-PL) [67]. In HepG2 cell line cytotoxic effect of low concentrations (IC_{50} after 24 h incubation – 13.49 μg mL^{-1}) has been reported for ε-PL. In L-02 cell line, a reduction in cell viability by up to 40% was observed for ε-PL concentration equal to 64 μg mL^{-1} [68], overall leading to the fact that IC_{50} value depends on the cell phenotype.

3.3.2. *Cytotoxicity of hydrogel samples*

The fabricated HA/ε-PL hydrogel samples were then evaluated in both direct contact assay (Fig. 7B–D) and indirect (extract) tests (Fig. 8A–C). The phys HA/ε-PL hydrogels had a negative effect on the cell viability in the direct cytotoxicity test – all hydrogel samples reduced viability by more than 50% (Fig. 7B). The effect was statistically significant compared to untreated control, but no differences were observed between the phys HA/ε-PL hydrogels of different HA to ε-PL mass ratios (Fig. 7B). The microscopic evaluation showed reduced cell confluence and changed morphology in the presence of the phys HA/ε-PL hydrogels (Fig. 7D c–e). The chem HA/ε-PL hydrogels had a little effect on cell viability in the direct cytotoxicity test (Fig. 7C). By the microscopic evaluation, cells grew and showed normal morphology when cultivated in direct contact with the chem HA/ε-PL hydrogels (Fig. 7D f–h).

Indirect cytotoxicity test showed that extracts of the Phys HA/ε-PL hydrogel samples at the tested concentrations of 12.5%, 25%, 50% (v/v) had a negative or moderate negative effect on cell viability. The extracts of the Phys HA/ε-PL 40:60 hydrogel samples exhibited the most pronounced toxic effect compared to the other two samples (Fig. 8A). Moreover, cell viability was improved at the lower extract concentrations of 12.5% (v/v) for the Phys HA/ε-PL hydrogels (Fig. 8A, C). Among the chem HA/ε-PL hydrogels, the least toxic effect was observed for the chem HA/ε-PL 40:60 samples – at 50% (v/v) extract reduced cell viability by 13.5% (Fig. 8B). Moreover, by the lower extract concentrations of 12.5% and 25% (v/v) for chem HA/ε-PL hydrogels, cell viability was close to the untreated control level or slightly exceeded it (Fig. 8B). However, the microscopic evaluation revealed lower cell density than the untreated control (Fig. 8C). The extract concentration of 50% (v/v) of chem HA/ε-PL 50:50 and chem HA/ε-PL 60:40 samples reduced cell viability by 50% and 86%, respectively (Fig. 8B). Overall, the indirect (extract) test results showed similar trends as the direct test results of the chem HA/ε-PL hydrogels (Fig. 7C, D). Cytotoxicity assessment of the Phys HA/ε-PL hydrogels by both direct contact (Fig. 7B, D) and indirect (extract) (Fig. 8A, C) tests showed that the phys HA/ε-PL hydrogel samples with higher antimicrobial activity (Fig. 6,

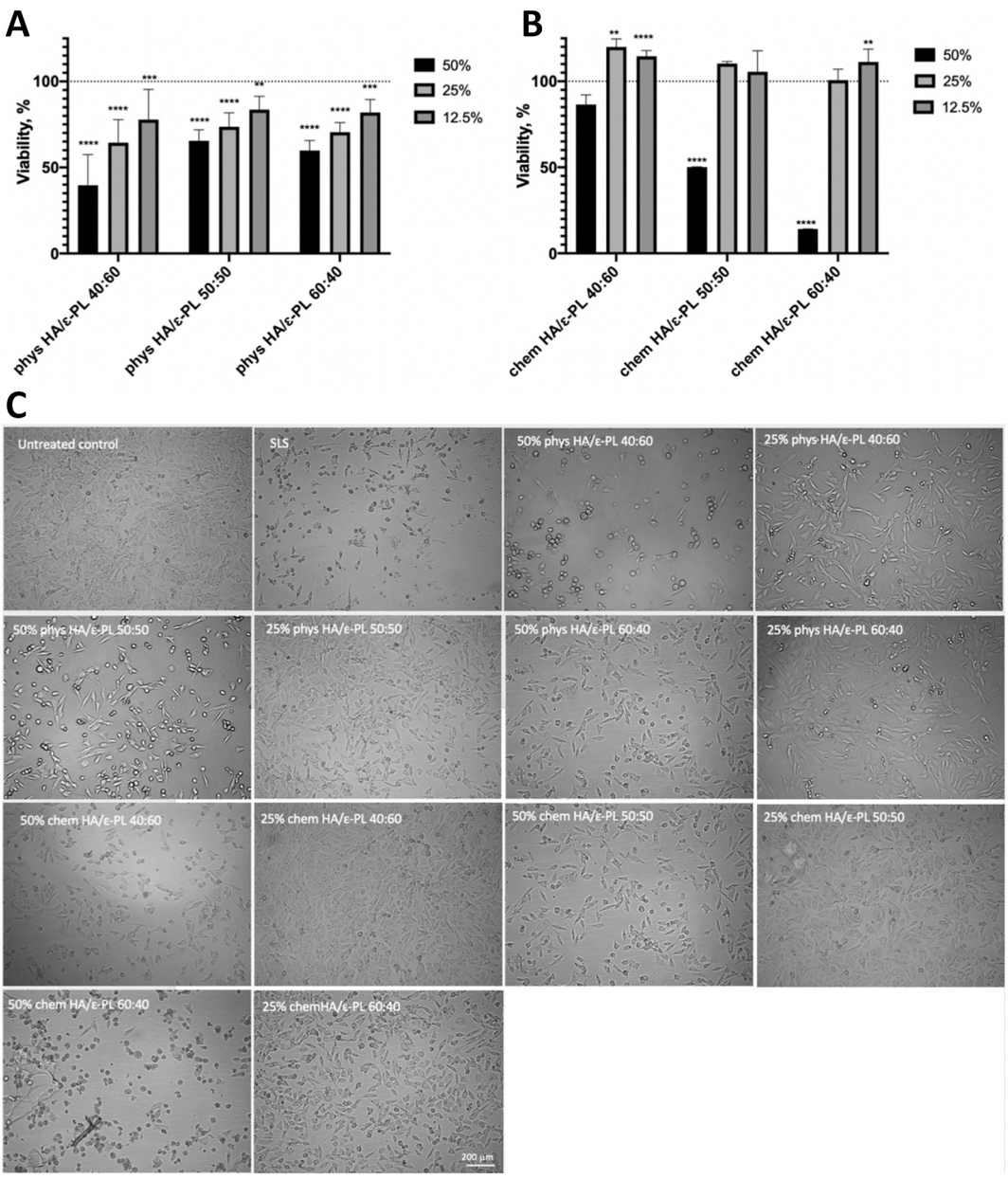

Fig. 8. (A) Cell viability after 24 h incubation with extracts of the phys HA/ε-PL hydrogels (B) and extracts of the chem HA/ε-PL hydrogels. Dashed line indicates untreated control level (100%). (C) Representative images of BALB/c 3T3 cells after 24 h incubation with the phys and chem HA/ε-PL hydrogel extracts at 50% and 25% (v/v). SLS- sodium lauryl sulfate (cytotoxicity control); $n = 5$ (for phys samples), $n = 4$ (for chem samples at 50% and 25% (v/v)) $n = 9$ (for chem samples at 12.5% (v/v)); mean ± SD; ** - $p < 0.01$; *** - $p < 0.001$; **** - $p < 0.0001$).

Table 2) had adverse effects on mammalian cell viability. In the case of the chem HA/ε-PL hydrogels, reduced cell viability was observed when extracts were tested (Fig. 8B). The increased cytotoxicity effect was found for the chem HA/ε-PL 60:40 hydrogels (Fig. 8B). We hypothesize that this effect occurred due to the release of residual non-crosslinked ε-PL primary amino groups from the hydrogel and could be supported by the highest swelling degree of chem HA/ε-PL 60:40 samples (Fig. 3B). Extracts were tested in 24-well plates with lower cultivation media volume and total seeded cell number than that used in 6-well plates performing direct contact test. This might explain the deviations between the direct and extract test results. It should be noted that in several studies where good biocompatibility of ε-PL containing composites has been shown, ε-PL concentrations lower than those used in the current study were applied [17,66,69]. On the other hand, HA as a bioactive component for tissue engineering applications is widely investigated and is considered non-cytotoxic, and shows good biocompatibility [70]. However, slight changes in cell viability have been observed in different cell lines when different HA-containing materials were assayed for cytotoxicity [71,72]. As the antimicrobial activity of hydrogels is attributable to ε-PL ability to permeabilize and disrupt the cell membranes, interactions with mammalian cell membranes might be the underlying mechanism for the composite hydrogel toxicity. Thus, further biocompatibility studies should be performed to elucidate specific effects of the fabricated Phys and chem HA/ε-PL hydrogels on cell viability, proliferation, migration, and functionality.

4. Conclusions

In this study, a series of physical and chemical crosslinked hyaluronic acid (HA)/ε-polylysine (ε-PL) hydrogels with HA to ε-PL mass ratio of 40:60 wt%, 50:50 wt%, 60:40 wt% (corresponding to molar ratios of 1:600, 1:400 and 1:270, respectively) have been prepared. The impact of

the crosslinking strategy on the physicochemical properties, antibacterial activity, and in vitro biocompatibility was evaluated. Obtained results revealed the significant impact of the crosslinking strategy on the swelling behavior, gel fraction, fast-acting antibacterial activity, and cytotoxicity of the fabricated hydrogels. The physically crosslinked hydrogels were prepared at significantly higher HA concentrations (16–24 wt%), 4-fold higher than chemically prepared gels at 5.25 wt% HA content, allowing them to exhibit similar order of magnitude of stiffness (10–30 kPa). Higher content of free charged NH_3^+ groups presented in the physically crosslinked hydrogels compared to the chemically crosslinked ones was confirmed by Fourier transform infrared spectroscopy. As such, the physically crosslinked hydrogels demonstrated a superior inhibitory effect (99.999%) on Gram-negative *E. coli*. While the chemically crosslinked hydrogels had a significantly lower inhibitory effect, related to the amount of available free charged NH_3^+ groups, lower polymer concentration, and the chemical modification directly involves NH_2 groups in covalent crosslinking, impairing its exposition and action to bacteria.

Furthermore, the obtained data confirmed the cytotoxicity of ε-PL at concentrations over 3.91 mg mL^{-1}, while this concentration was found to be favorable for antimicrobial activity. According to the cell viability tests, the chemically crosslinked hydrogels revealed superior cytocompatibility than the physically crosslinked hydrogels. The highest cell viability was observed for the chemically crosslinked HA/ε-PL 40:60 hydrogels and the physically crosslinked HA/ε-PL 60:40 hydrogel samples. Differences in the binding of amino groups of ε-PL in the physically and chemically crosslinked HA/ε-PL hydrogels and the release rate of these groups can explain the disparities in antibacterial activity and cell viability. The hypothesis that the release profile of primary amino groups of ε-PL from the fabricated HA/ε-PL hydrogels is responsible for the antibacterial and cytocompatibility performance will be tested in further studies. The distinct differences in biological and antibacterial properties of the developed chemically and physically crosslinked hydrogels provide new opportunities for the next generation functional biomaterial systems.

Supplementary data to this article can be found online at https://doi.org/10.1016/j.ijbiomac.2022.03.207.

CRediT authorship contribution statement

Kristine Salma-Arcane: Conceptualization, Supervision, Resources, Writing- Original draft preparation, Methodology, Validation, Writing - Review & Editing. **Artemis Sceglovs**: Methodology, Validation, Formal analysis, Investigation. **Eliza Trauma**: Methodology, Validation, Formal analysis, Investigation. **Jacek K. Wychowaniec**: Writing - Review & Editing, Methodology, Validation, Formal analysis, Investigation, Supervision. **Kristine Aunina**: Methodology, Validation, Formal analysis, Investigation. **Anna Ramata-Stunda**: Writing- Original draft preparation, Methodology, Validation, Formal analysis, Investigation. **Visma Nikolajeva**: Writing- Original draft preparation, Methodology, Validation, Formal analysis, Investigation. **Dagnija Loca**: Conceptualization, Supervision, Resources, Writing- Original draft preparation, Methodology, Writing - Review & Editing, Funding acquisition.

Declaration of competing interest

None.

Acknowledgements

The authors acknowledge financial support from the Latvian Council of Science research project No. lzp-2019/1-0005 "Injectable *in situ* self-crosslinking composite hydrogels for bone tissue regeneration (iBone)" and European Union's Horizon 2020 research and innovation programme under the grant agreement No. 952347 (RISEus2). J. K. W. gratefully acknowledges the European Union's Horizon 2020 (H2020-MSCA-IF-2019) research and innovation programme under the Marie Skłodowska-Curie grant agreement 893099 — ImmunoBioInks.

References

[1] D.L. Kusindarta, H. Wihadmadyatami, The Role of Extracellular Matrix in Tissue Regeneration, INTECH, 2018, https://doi.org/10.5772/intechopen.75728.
[2] J. Nicolas, L. Rabbachin, S. Sampaolesi, F. Nicotra, L. Russo, 3D extracellular matrix mimics: fundamental concepts and role of materials chemistry to influence stem cell fate, Biomacromolecules 21 (6) (2020) 1968–1994, https://doi.org/10.1021/acs.biomac.0c00045.
[3] S. Amorim, C.A. Reis, R.L. Reis, R.A. Pires, Extracellular matrix mimics using hyaluronan-based biomaterials, Trends Biotechnol. 39 (1) (2021) 90–104, https://doi.org/10.1016/j.tibtech.2020.06.003.
[4] S. Vigier, T. Fülöp, Exploring the Extracellular Matrix to Create Biomaterials, INTECH, 2016, https://doi.org/10.5772/62979.
[5] G. Jose, K.T. Shalumon, J. Chen, Natural polymers based hydrogels for cell culture applications, Curr. Med. Chem. 27 (16) (2020) 2734–2776, https://doi.org/10.2174/0929867326666190903113004.
[6] A. Vedadghavami, F. Minooei, M.H. Mohammadi, S. Khetani, A. Rezaei Kolahchi, S. Mashayekhan, A. Sanati-Nezhad, Manufacturing of hydrogel biomaterials with controlled mechanical properties for tissue engineering applications, Acta Biomater. 62 (2017) 42–63, https://doi.org/10.1016/j.actbio.2017.07.028.
[7] X. Bai, M. Gao, S. Syed, J. Zhuang, X. Xu, X. Zhang, Bioactive hydrogels for bone regeneration, Bioact. Mater. 3 (4) (2018) 401–417, https://doi.org/10.1016/j.bioactmat.2018.05.006.
[8] C.D.F. Moreira, S.M. Carvalho, R.M. Florentino, A. França, B.S. Okano, C.M. F. Rezende, H.S. Mansur, M.M. Pereira, Injectable chitosan/gelatin/bioactive glass nanocomposite hydrogels for potential bone regeneration. In vitro and in vivo analyses, Int. J. Biol. Macromol. 132 (2019) 811–821, https://doi.org/10.1016/j.ijbiomac.2019.03.237.
[9] D. Harrer, E. Sanchez Armengol, J.D. Friedl, A. Jalil, M. Jelkmann, C. Leichner, F. Laffleur, Is hyaluronic acid the perfect excipient for the pharmaceutical need? Int. J. Pharm. 601 (2021), 120589 https://doi.org/10.1016/j.ijpharm.2021.120589.
[10] W. Guo, L. Douma, M.H. Hu, D. Eglin, M. Alini, A. Šećerović, S. Grad, X. Peng, X. Zou, M. D'Este, Hyaluronic acid-based interpenetrating network hydrogel as a cell carrier for nucleus pulposus repair, Carbohydr. Polym. 277 (2022), 118828, https://doi.org/10.1016/j.carbpol.2021.118828.
[11] N.A. El-Sersy, A.E. Abdelwahab, S.S. Abouelkhiir, D.M. Abou-Zeid, S.A. Sabry, Antibacterial and anticancer activity of ε-poly-L-lysine (ε -PL) produced by a marine Bacillus subtilis sp. J. Basic Microbiol. 52 (5) (2012) 513–522, https://doi.org/10.1002/jobm.201100290.
[12] L. Cai, S. Liu, J. Guo, Y. Jia, Polypeptide-based self-healing hydrogels: design and biomedical applications, Acta Biomater. 113 (2020) 84–100, https://doi.org/10.1016/j.actbio.2020.07.001.
[13] S. Chen, S. Huang, Y. Li, C. Zhou, Recent advances in epsilon-poly-L-lysine and L-lysine-based dendrimer synthesis, modification, and biomedical applications, Front. Chem. 9 (2021), 659304, https://doi.org/10.3389/fchem.2021.659304.
[14] N.A. Patil, B. Kandasubramanian, Functionalized polylysine biomaterials for advanced medical applications: a review, Eur. Polym. J. 146 (2021), 110248, https://doi.org/10.1016/j.eurpolymj.2020.110248.
[15] R. Wang, B. Zhou, D. Xu, H. Xu, L. Liang, X. Feng, P. Ouyang, B. Chi, Antimicrobial and biocompatible ε-polylysine–γ-poly(glutamic acid)–based hydrogel system for wound healing, J. Bioact. Compat. Polym. 31 (3) (2016) 242–259, https://doi.org/10.1177/0883911515610019.
[16] S. Li, S. Dong, W. Xu, S. Tu, L. Yan, C. Zhao, J. Ding, X. Chen, Antibacterial hydrogels, Adv. Sci. 1700527 (2018), https://doi.org/10.1002/advs.201700527.
[17] R. Wang, D. Xu, L. Liang, T. Xu, W. Liu, P. Ouyang, B. Chi, H. Xu, Enzymatically crosslinked epsilon-poly-L-lysine hydrogels with inherent antibacterial properties for wound infection prevention, RSC Adv. 6 (11) (2016) 8620–8627, https://doi.org/10.1039/C5RA15616E.
[18] W. Hu, Z. Wang, Y. Xiao, S. Zhang, J. Wang, Advances in crosslinking strategies of biomedical hydrogels, Biomater. Sci. 7 (3) (2019) 843–855, https://doi.org/10.1039/C8BM01246F.
[19] H. Cui, X. Zhuang, C. He, Y. Wei, X. Chen, High performance and reversible ionic polypeptide hydrogel based on charge-driven assembly for biomedical applications, Acta Biomater. 11 (2015) 183–190, https://doi.org/10.1016/j.actbio.2014.09.017.
[20] X. Xue, Y. Hu, S. Wang, X. Chen, Y. Jiang, J. Su, Fabrication of physical and chemical crosslinked hydrogels for bone tissue engineering, Bioact. Mater. (October) (2021), https://doi.org/10.1016/j.bioactmat.2021.10.029.
[21] J.H. Lee, Injectable hydrogels delivering therapeutic agents for disease treatment and tissue engineering, Biomater. Res. 22 (1) (2018) 27, https://doi.org/10.1186/s40824-018-0138-6.
[22] N. Reddy, R. Reddy, Q. Jiang, Crosslinking biopolymers for biomedical applications, Trends Biotechnol. 33 (6) (2015) 362–369, https://doi.org/10.1016/j.tibtech.2015.03.008.
[23] S. Dakhara, C. Anajwala, Polyelectrolyte complex: a pharmaceutical review, Syst. Rev. Pharm. 1 (2) (2010) 121–127, https://doi.org/10.4103/0975-8453.75046.
[24] J. Lv, Y. Meng, Y. Shi, Y. Li, J. Chen, F. Sheng, Properties of epsilon-polylysine•HCl/high-methoxyl pectin polyelectrolyte complexes and their commercial application, J. Food Process. Preserv. 44 (2) (2020), e14320, https://doi.org/10.1111/jfpp.14320.

[25] M.P. Wickramathilaka, B.Y. Tao, Characterization of covalent crosslinking strategies for synthesizing DNA-based bioconjugates, J. Biol. Eng. 13 (1) (2019) 63, https://doi.org/10.1186/s13036-019-0191-2.
[26] J. Hua, Z. Li, W. Xia, N. Yang, J. Gong, J. Zhang, C. Qiao, Preparation and properties of EDC/NHS mediated crosslinking poly (gamma-glutamic acid)/epsilon-polylysine hydrogels, Mater. Sci. Eng. C 61 (2016) 879–892, https://doi.org/10.1016/j.msec.2016.01.001.
[27] J. Ahn, L. Kuffova, K. Merrett, D. Mitra, J.V. Forrester, F. Li, M. Griffith, Crosslinked collagen hydrogels as corneal implants: effects of sterically bulky vs. non-bulky carbodiimides as crosslinkers, Acta Biomater. 9 (8) (2013) 7796–7805, https://doi.org/10.1016/j.actbio.2013.04.014.
[28] J.Y. Seo, B. Lee, T.W. Kang, J.H. Noh, M.J. Kim, Y.B. Ji, H.J. Ju, B.H. Min, M. S. Kim, Electrostatically interactive injectable hydrogels for drug delivery, Tissue Eng. Regen. Med. 15 (5) (2018) 513–520, https://doi.org/10.1007/s13770-018-0146-6.
[29] M. He, L. Shi, G. Wang, Z. Cheng, L. Han, X. Zhang, C. Wang, J. Wang, P. Zhou, G. Wang, Biocompatible and biodegradable chitosan/sodium polyacrylate polyelectrolyte complex hydrogels with smart responsiveness, Int. J. Biol. Macromol. 155 (2020) 1245–1251, https://doi.org/10.1016/j.ijbiomac.2019.11.092.
[30] M.E. van Gent, M. Ali, P.H. Nibbering, S.N. Kłodzińska, Current advances in lipid and polymeric antimicrobial peptide delivery systems and coatings for the prevention and treatment of bacterial infections, Pharmaceutics 13 (11) (2021) 1840, https://doi.org/10.3390/pharmaceutics13111840.
[31] Y. Chang, L. McLandsborough, D.J. McClements, Antimicrobial delivery systems based on electrostatic complexes of cationic Ɛ-polylysine and anionic gum arabic, Food Hydrocoll. 35 (2014) 137–143, https://doi.org/10.1016/j.foodhyd.2013.05.004.
[32] V.Z. Prokopović, C. Duschl, D. Volodkin, Hyaluronic acid/poly-l-lysine multilayers as seservoirs for storage and release of small charged molecules, Macromol. Biosci. 15 (10) (2015) 1357–1363, https://doi.org/10.1002/mabi.201500093.
[33] E. Tračuma, D. Loca, Hyaluronic acid/polylysine composites for local drug delivery: a review, Key Eng. Mater. 850 (2020) 213–218, https://doi.org/10.4028/www.scientific.net/KEM.850.213.
[34] Y. Zou, S. He, J. Du, ε-Poly(L-lysine)-based hydrogels with fast-acting and prolonged antibacterial activities, Chin. J. Polym. Sci. 36 (11) (2018) 1239–1250, https://doi.org/10.1007/s10118-018-2156-1.
[35] R. Wang, B. Zhou, W. Liu, X. Feng, S. Li, D. Yu, J. Chang, B. Chi, H. Xu, Fast in situ generated Ɛ-polylysine-poly (ethylene glycol) hydrogels as tissue adhesives and hemostatic materials using an enzyme-catalyzed method, J. Biomater. Appl. 29 (8) (2015) 1167–1179, https://doi.org/10.1177/0885328214553960.
[36] L. Stipniece, K. Salma-Ancane, I. Narkevica, I. Juhnevica, L. Berzina-Cimdina, Fabrication of nanostructured composites based on hydroxyapatite and ε-polylysine, Mater. Lett. 163 (2016) 65–68, https://doi.org/10.1016/j.matlet.2015.10.077.
[37] S.C. Shukla, A. Singh, A.K. Pandey, A. Mishra, Review on production and medical applications of ε-polylysine, Biochem. Eng. J. 65 (2012) 70–81, https://doi.org/10.1016/j.bej.2012.04.001.
[38] A. Ščeglovs, K. Salma-Ancane, Novel hydrogels and composite hydrogels based on ε-polylysine, hyaluronic acid and hydroxyapatite, Key Eng. Mater. 850 (1) (2020) 242–248, https://doi.org/10.4028/www.scientific.net/KEM.850.242.
[39] A. Ström, A. Larsson, O. Okay, Preparation and physical properties of hyaluronic acid-based cryogels, J. Appl. Polym. Sci. 132 (29) (2015) 42194, https://doi.org/10.1002/app.42194.
[40] R. Gilli, M. Kacuráková, M. Mathlouthi, L. Navarini, S. Paoletti, FTIR studies of sodium hyaluronate and its oligomers in the amorphous solid phase and in aqueous solution, Carbohydr. Res. 263 (2) (1994) 315–326, https://doi.org/10.1016/0008-6215(94)00147-2.
[41] K. Haxaire, Y. Maréchal, M. Milas, M. Rinaudo, Hydration of polysaccharide hyaluronan observed by IR spectrometry. I. Preliminary experiments and band assignments, Biopolymers 72 (1) (2003) 10–20, https://doi.org/10.1002/bip.10245.
[42] M. Rozenberg, G. Shoham, FTIR spectra of solid poly-l-lysine in the stretching NH mode range, Biophys. Chem. 125 (1) (2007) 166–171, https://doi.org/10.1016/j.bpc.2006.07.008.
[43] J. Chen, H. Liu, Z. Xia, X. Zhao, Y. Wu, M. An, Purification and structural analysis of the effective anti-TMV compound ε-poly-l-lysine produced by Streptomyces ahygroscopicus, Molecules 24 (6) (2019) 1156, https://doi.org/10.3390/molecules24061156.
[44] R.A. Sequeira, N. Singh, M.M. Pereira, N.A. Chudasama, S. Bhattacharya, M. Sharma, D. Mondal, K. Prasad, High concentration solubility and stability of ε-poly-l-lysine in an ammonium-based ionic liquid: a suitable media for polypeptide packaging and biomaterial preparation, Int. J. Biol. Macromol. 120 (2018) 378–384, https://doi.org/10.1016/j.ijbiomac.2018.08.102.
[45] A. Barth, The infrared absorption of amino acid side chains, Prog. Biophys. Mol. Biol. 74 (3–5) (2000) 141–173, https://doi.org/10.1016/S0079-6107(00)00021-3.
[46] A. Barth, Infrared spectroscopy of proteins, Biochim. Biophys. Acta - Bioenerg. 1767 (9) (2007) 1073–1101, https://doi.org/10.1016/j.bbabio.2007.06.004.
[47] K. Yang, Q. Han, B. Chen, Y. Zheng, K. Zhang, Q. Li, J. Wang, Antimicrobial hydrogels: promising materials for medical application, Int. J. Nanomedicine 13 (2018) 2217–2263, https://doi.org/10.2147/IJN.S154748.
[48] X. Zhang, M. Qin, M. Xu, F. Miao, C. Merzougui, X. Zhang, Y. Wei, W. Chen, D. Huang, The fabrication of antibacterial hydrogels for wound healing, Eur. Polym. J. 146 (2021), 110268, https://doi.org/10.1016/j.eurpolymj.2021.110268.
[49] P. Zhai, X. Peng, B. Li, Y. Liu, H. Sun, X. Li, The application of hyaluronic acid in bone regeneration, Int. J. Biol. Macromol. 151 (2019) 1224–1239, https://doi.org/10.1016/j.ijbiomac.2019.10.169.
[50] M.J. Zohuriaan-Mehr, A. Pourjavadi, H. Salimi, M. Kurdtabar, Protein- and homo poly(amino acid)-based hydrogels with super-swelling properties, Polym. Adv. Technol. 20 (8) (2009) 655–671, https://doi.org/10.1002/pat.1395.
[51] Y. Xue, H. Chen, C. Xu, D. Yu, H. Xu, Y. Hu, Synthesis of hyaluronic acid hydrogels by crosslinking the mixture of high-molecular-weight hyaluronic acid and low-molecular-weight hyaluronic acid with 1,4-butanediol diglycidyl ether, RSC Adv. 10 (12) (2020) 7206–7213, https://doi.org/10.1039/C9RA09271D.
[52] C.E. Schanté, G. Zuber, C. Herlin, T.F. Vandamme, Chemical modifications of hyaluronic acid for the synthesis of derivatives for a broad range of biomedical applications, Carbohydr. Polym. 85 (3) (2011) 469–489, https://doi.org/10.1016/j.carbpol.2011.03.019.
[53] D. Eyrich, F. Brandl, B. Appel, H. Wiese, G. Maier, M. Wenzel, R. Staudenmaier, A. Goepferich, T. Blunk, Long-term stable fibrin gels for cartilage engineering, Biomaterials 28 (1) (2007) 55–65, https://doi.org/10.1016/j.biomaterials.2006.08.027.
[54] R.A. Batista, P.J.P. Espitia, D.M.C. Vergne, A.A. Vicente, P.A.C. Pereira, M. A. Cerqueira, J.A. Teixeira, J. Jovanovic, P. Severino, E.B. Souto, Development and evaluation of superabsorbent hydrogels based on natural polymers, Polymers (Basel) 12 (10) (2020) 2173, https://doi.org/10.3390/polym12102173.
[55] C.M. Walsh, J.K. Wychowaniec, D.F. Brougham, D. Dooley, Functional hydrogels as therapeutic tools for spinal cord injury: new perspectives on immunopharmacological interventions, Pharmacol. Ther. 108043 (2021), https://doi.org/10.1016/j.pharmthera.2021.108043.
[56] J.K. Wychowaniec, J. Litowczenko, K. Tadyszak, V. Natu, C. Aparicio, B. Peplińska, M.W. Barsoum, M. Otyepka, B. Scheibe, Unique cellular network formation guided by heterostructures based on reduced graphene oxide - Ti3C2Tx MXene hydrogels, Acta Biomater. 115 (2020) 104–115, https://doi.org/10.1016/j.actbio.2020.08.010.
[57] A. Dodero, R. Williams, S. Gagliardi, S. Vicini, M. Alloisio, M.A. Castellano, Micro-rheological and rheological study of biopolymers solutions: hyaluronic acid, Carbohydr. Polym. 203 (2019) 349–355, https://doi.org/10.1016/j.carbpol.2018.09.072.
[58] J.M. Guenet, Thermoreversible Gelation of Polymers and Biopolymers, Academic Press, 1992.
[59] J.M. Guenet, Organogels. Thermodynamics, Structure, Solvent Role, and Properties, Springer International Publishing, Cham, 2016, https://doi.org/10.1007/978-3-319-33178-2.
[60] J.K. Wychowaniec, M. Iliut, M. Zhou, J. Moffat, M.A. Elsawy, W.A. Pinheiro, J. A. Hoyland, A.F. Miller, A. Vijayaraghavan, A. Saiani, Designing peptide/graphene hybrid hydrogels through fine-tuning of molecular interactions, Biomacromolecules 19 (7) (2018) 2731–2741, https://doi.org/10.1021/acs.biomac.8b00333.
[61] T. Yoshida, T. Nagasawa, Epsilon-poly-l-lysine: microbial production, biodegradation and application potential, Appl. Microbiol. Biotechnol. 62 (1) (2003) 21–26, https://doi.org/10.1007/s00253-003-1312-9.
[62] Z. Tan, Y. Shi, B. Xing, Y. Hou, J. Cui, S. Jia, The antimicrobial effects and mechanism of ε-poly-lysine against Staphylococcus aureus, Bioresour. Bioprocess. 6 (1) (2019) 11, https://doi.org/10.1186/s40643-019-0246-8.
[63] Y. Li, Q. Han, J. Feng, W. Tian, H. Mo, Antibacterial characteristics and mechanisms of Ɛ-poly-lysine against Escherichia coli and Staphylococcus aureus, Food Control 43 (2014) 22–27, https://doi.org/10.1016/j.foodcont.2014.02.023.
[64] K. Ushimaru, T. Morita, T. Fukuoka, Bio-based, flexible, and tough material derived from ε-poly-l-lysine and fructose via the Maillard reaction, ACSOmega 5 (36) (2020) 22793–22799, https://doi.org/10.1021/acsomega.0c01813.
[65] A. Sun, X. He, L. Li, T. Li, Q. Liu, X. Zhou, X. Ji, W. Li, Z. Qian, An injectable photopolymerized hydrogel with antimicrobial and biocompatible properties for infected skin regeneration, NPG Asia Mater. 12 (1) (2020) 25, https://doi.org/10.1038/s41427-020-0206-y.
[66] C. Zhou, P. Li, X. Qi, A.R.M. Sharif, Y.F. Poon, Y. Cao, M.W. Chang, S.S.J. Leong, M. B. Chan-Park, A photopolymerized antimicrobial hydrogel coating derived from epsilon-poly-l-lysine, Biomaterials 32 (11) (2011) 2704–2712, https://doi.org/10.1016/j.biomaterials.2010.12.040.
[67] S. Hyon, N. Nakajima, H. Sugai, K. Matsumura, Low cytotoxic tissue adhesive based on oxidized dextran and epsilon-poly-L-lysine, J. Biomed. Mater. Res. Part A 102 (8) (2014) 2511–2520, https://doi.org/10.1002/jbm.a.34923.
[68] C. Shi, X. Zhao, Z. Liu, R. Meng, X. Chen, N. Guo, Antimicrobial, antioxidant, and antitumor activity of epsilon-poly-L-lysine and citral, alone or in combination, Food Nutr. Res. 60 (1) (2016) 31891, https://doi.org/10.3402/fnr.v60.31891.
[69] F. Wahid, F. Wang, Y. Xie, L. Chu, S. Jia, Y. Duan, L. Zhang, C. Zhong, Reusable ternary PVA films containing bacterial cellulose fibers and ε-polylysine with improved mechanical and antibacterial properties, Colloids Surf. B Biointerfaces 183 (September) (2019), 110486, https://doi.org/10.1016/j.colsurfb.2019.110486.
[70] J. Necas, L. Bartosikova, P. Brauner, J. Kolar, Hyaluronic acid (hyaluronan): a review, Vet. Med. (Praha) 53 (8) (2008) 397–411, https://doi.org/10.17221/1930-VETMED.
[71] D.G. Boeckel, R.S.A. Shinkai, M.L. Grossi, E.R. Teixeira, In vitro evaluation of cytotoxicity of hyaluronic acid as an extracellular matrix on OFCOL II cells by the MTT assay, Oral Surg.Oral Med. Oral Pathol. Oral Radiol. 117 (6) (2014) e423–e428, https://doi.org/10.1016/j.oooo.2012.07.486.
[72] S. Gedikli, G. Güngör, Y. Toptaş, D.E. Sezgin, M. Demirbilek, N. Yazıhan, P. Aytar Çelik, E.B. Denkbaş, V. Bütün, A. Çabuk, Optimization of hyaluronic acid production and its cytotoxicity and degradability characteristics, Prep. Biochem.

Biotechnol. 48 (7) (2018) 610–618, https://doi.org/10.1080/10826068.2018.1476885.